

# Direct calculation of the electrode movement Jacobian for 3D EIT

Camille Gómez-Laberge<sup>1</sup> and Andy Adler<sup>1</sup>

<sup>1</sup>Systems and Computer Engineering, Carleton University, Ottawa, Canada

**Abstract**—Electrical Impedance Tomography (EIT) of media with deformable boundaries is very sensitive to electrode movement. This is especially important for EIT images of the thorax, which become distorted with breathing and posture change. Previously, we proposed a reconstruction method for imaging conductivity change and electrode movement based on an indirect perturbation Jacobian calculation, involving the re-computation of the forward solution. Although suitable for 2D and small 3D imaging, the reconstruction accuracy of this method gradually decreases, while the computation time grows rapidly for large 3D problems. We propose an efficient, novel method of calculating the Jacobian matrix directly from the Finite Element Method (FEM) system equations, without the re-calculation of the forward solution.

The implemented algorithm is based on asymmetric rank-one perturbations of the admittance matrix. We show that the measurement sensitivity calculations, due to the displacement of each electrode, reduce to operations on small submatrices of the FEM system matrix. The proposed algorithm is applied to simulated data using 3D FEM reconstruction models of various element densities. The computation speed and the reconstruction fidelity are compared between the proposed and previous methods.

**Keywords**—electrical impedance tomography, electrode movement, inverse problems.

## I. INTRODUCTION

In clinical EIT, boundary deformation occurs mostly in thoracic measurement due to breathing and posture change during measurement [1]. The former causes the expansion and the contraction of the rib cage; the latter causes a displacement of the skin and the electrodes with respect to the lungs. The difficulty arises since EIT measurements are imposed onto a geometric reconstruction model that approximates the shape of the body being observed. The movement of electrodes reduces the accuracy of the reconstruction model and introduces spurious difference measurements producing broad artefacts in the images [2]. Related are the errors from inadequate geometric models and inconsistent electrode placement. These problems are well known in the literature.

Blott *et al.* studied the effects of electrode movement in 2D EIT and compensated for reconstruction error by re-adjusting measurement data using a spatial smoothness

constraint [3]. Lionheart showed that in 3D EIT, the measurement data is sufficient to determine both the conductivity distribution and the boundary shape [4]. In order to attempt accounting for the errors due to electrode movement, EIT imaging algorithms have been developed to reconstruct both the conductivity change and the electrode movement [5], [6]. These approaches are promising and show dramatic decreases in image artefacts associated with electrode movement. One limitation of these techniques is that the Jacobian (or sensitivity) matrix needs to be calculated for both conductivity change and electrode movement. While good algorithms for the conductivity change Jacobian are available [7], the electrode movement portion has been calculated using numerical perturbation techniques. This computation is slow and can be numerically inaccurate as the FEM models get larger. This article proposes an efficient method of *directly* calculating the Jacobian matrix, i.e., without using numerical perturbation and re-calculation of the forward problem.

## II. METHODS

### A. The system model

The conductivity distribution is represented within the 3D FEM volume. The FEM used in this paper is constructed by extruding a 2D circular FEM into a 3D cylinder with tetrahedral elements. The conductivity distribution is constant on each element, and is defined as the vector  $\sigma \in \mathbb{R}^{N_k}$ , where  $N_k$  is the number of elements in the FEM.

Sixteen electrodes are placed around the volume's circumference in correspondence with the experiment's electrode configuration. Point electrodes are considered, which are directly connected to the nodes on the 3D model boundary. Figure 1 illustrates a 7,680-element FEM model with the electrode configuration used in this paper. The electrodes are numbered in a “zig-zag” pattern [8], where electrode 1 (light), electrode 2 (medium), and the remaining electrodes (dark) are shown by green stars in figure 1. The potential difference between electrode  $i$  and the reference is defined as  $\phi_i$ . The two blue elements shown in figure 1 are contrast elements used to compare image reconstructions. While two electrodes excite the medium, the remaining

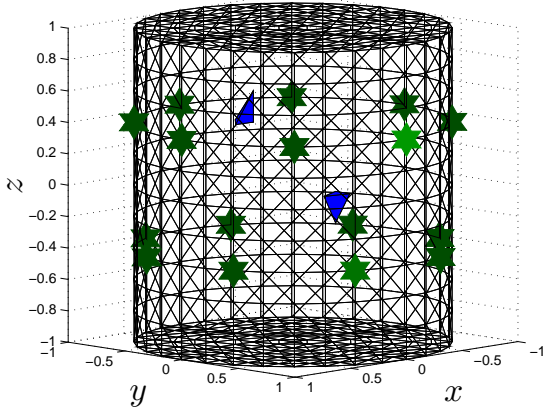


Fig. 1 A forward model FEM with 7,680 tetrahedral elements.

electrodes measure the voltage between adjacent pairs. The  $k^{\text{th}}$  measurement  $v_k = \phi_i - \phi_j$ , is the voltage between two electrodes  $i$  and  $j$ . This excitation process is repeated for each electrode pair; therefore, for  $N_e$  electrodes, we obtain  $N_v = N_e(N_e - 3)$  voltage measurements  $\mathbf{v} \in \mathbb{R}^{N_v}$ .

In the forward problem, we also consider each electrode's position vector  $\mathbf{r} \in \mathbb{R}^3$ , since we expect displacements to occur during the measurements. Hence,  $\boldsymbol{\sigma}$  and  $\mathbf{r}$  are used to construct the *admittance matrix*  $\mathbf{Y} \in \mathbb{R}^{N_p \times N_p}$ , where  $N_p$  is the number of nodes in the FEM. This matrix associates each FEM element  $i = 1, \dots, N_k$  to its conductivity  $\sigma_i$  and its constituent nodes. The excitation pattern used to inject current into the medium is represented by the matrix  $\mathbf{Q} \in \mathbb{R}^{N_p \times N_e}$ . Each column of  $\mathbf{Q}$  indicates which electrodes are injecting current into the medium. The matrix product

$$\mathbf{V} = \mathbf{Y}(\boldsymbol{\sigma}, \mathbf{r})^{-1} \mathbf{Q} \quad (1)$$

yields the nodal potential difference matrix  $\mathbf{V} \in \mathbb{R}^{N_p \times N_e}$ , such that for excitation  $j = 1, \dots, N_e$ , we have  $\mathbf{V}_{ij} = \phi_i$  for nodes  $i = 1, \dots, N_p$ . Hence,  $\mathbf{v}$  can be extracted from  $\mathbf{V}$  by a series of element-wise subtractions  $\mathbf{V}_{ij} - \mathbf{V}_{kl}$  corresponding to the voltage measurement pattern. Although an extraction operator  $T$  is required to obtain  $\mathbf{v} = T[\mathbf{V}]$ , we omit this to simplify the formulation.

### B. Electrode movement Jacobian

The electrode movement Jacobian  $\mathbf{J}_m$  is a submatrix which augments the standard, conductivity Jacobian  $\mathbf{J}_c$ . Thus, the system matrix is formed as

$$\mathbf{J} = [\mathbf{J}_c, \mathbf{J}_m].$$

The conductivity Jacobian is calculated exactly as in [11] and has dimension  $\mathbb{R}^{N_v \times N_k}$ . This algorithm is available in the EIDORS software base under the GNU Public Licence [9]. By definition,  $\mathbf{J}_m$  is the sensitivity of the measurement data  $\mathbf{V}$  to the movement of an electrode with position vector  $\mathbf{r} = (r_x, r_y, r_z)$ . That is, for electrodes  $1, \dots, N_e$ , we have

$$\mathbf{J}_m = \left[ \frac{\partial \mathbf{V}}{\partial \mathbf{r}_1} \dots \frac{\partial \mathbf{V}}{\partial \mathbf{r}_{N_e}} \right] \in \mathbb{R}^{N_v \times 3N_e}. \quad (2)$$

Hence, we re-write the admittance matrix from equation (1) as a separable product

$$\mathbf{Y}(\boldsymbol{\sigma}, \mathbf{r}) = \mathbf{C}^\top \mathbf{D}(\boldsymbol{\sigma}) \mathbf{S}(\mathbf{r}) \mathbf{C}, \quad (3)$$

where  $\mathbf{C} \in \mathbb{R}^{N_k \times N_p}$  is the connectivity matrix, which associates each element to its vertices.  $\mathbf{D}(\boldsymbol{\sigma}) \in \mathbb{R}^{4N_k \times 4N_k}$  represents the conductivity distribution and is formed from

$$\mathbf{D}(\boldsymbol{\sigma}) = \text{diag}(\boldsymbol{\sigma}) \otimes \mathbf{I}_4 \quad (4)$$

where  $\otimes$  is the Kronecker product, and  $\mathbf{I}_4$  is the  $4 \times 4$  identity matrix. We refer to the matrix  $\mathbf{S}(\mathbf{r}) \in \mathbb{R}^{4N_k \times 4N_k}$  as the *FEM system matrix*, since it encapsulates the geometric properties of the FEM model. It is block-diagonal and defined as

$$\mathbf{S} = \begin{bmatrix} \mathbf{S}_1 & 0 & \dots & 0 \\ 0 & \mathbf{S}_2 & & \vdots \\ \vdots & & \ddots & 0 \\ 0 & \dots & 0 & \mathbf{S}_{N_k} \end{bmatrix}. \quad (5)$$

Each block is given by

$$\mathbf{S}_i = \frac{2}{N_d!} \frac{1}{|\det \mathbf{A}_i|} \mathbf{B}_i^\top \mathbf{B}_i,$$

where the model dimension  $N_d = 3$  for 3D. The matrix  $\mathbf{A}_i$  contains the geometry data of element  $i$

$$\mathbf{A}_i = \begin{bmatrix} 1 & r_x^1 & r_y^1 & r_z^1 \\ 1 & r_x^2 & r_y^2 & r_z^2 \\ 1 & r_x^3 & r_y^3 & r_z^3 \\ 1 & r_x^4 & r_y^4 & r_z^4 \end{bmatrix}^{-1}, \quad (6)$$

where  $(r_x^{j,i}, r_y^{j,i}, r_z^{j,i})$  is the  $(x, y, z)$  Cartesian co-ordinates of vertex  $j$  of element  $i$ . Each element  $i$ , is defined by its four vertices  $1 \leq j \leq 4$ . The matrix  $\mathbf{B}_i$  is the submatrix of  $\mathbf{A}_i$  with the top row deleted, denoted by  $\mathbf{B}_i = [\mathbf{A}_i]_{\setminus \text{row}1}$ .

In general, for an electrode with position vector  $\mathbf{r}$ , we have, from equations (1) and (2),

$$\frac{\partial \mathbf{V}}{\partial \mathbf{r}} = \frac{\partial}{\partial \mathbf{r}} \left( \mathbf{Y}^{-1} \mathbf{Q} \right) \quad (7)$$

$$= \mathbf{Y}^{-1} \frac{\partial \mathbf{Y}}{\partial \mathbf{r}} \mathbf{Y}^{-\top} \mathbf{Q}, \quad (8)$$

where, from equation (3),

$$\frac{\partial \mathbf{Y}}{\partial \mathbf{r}} = \mathbf{C}^\top \mathbf{D} \frac{\partial \mathbf{S}}{\partial \mathbf{r}} \mathbf{C}. \quad (9)$$

In order to evaluate equation (9), we need only consider the blocks  $\mathbf{S}_i$  where  $\mathbf{r}$  is a vertex node of the perturbed element  $i$ ; the other blocks vanish because they are constant. For each non-zero block, we require the derivative

$$\frac{\partial \mathbf{S}_i}{\partial \mathbf{r}} = \frac{\partial}{\partial \mathbf{r}} \left[ \frac{2}{N_d!} \frac{1}{|\det \mathbf{A}_i|} \mathbf{B}_i^\top \mathbf{B}_i \right].$$

The product rule of this equation yields

$$\begin{aligned} \frac{\partial \mathbf{S}_i}{\partial \mathbf{r}} &= \frac{2}{N_d!} \left[ \frac{\partial}{\partial \mathbf{r}} \left( \frac{1}{|\det \mathbf{A}_i|} \right) \mathbf{B}_i^\top \mathbf{B}_i + \right. \\ &\quad \left. \frac{1}{|\det \mathbf{A}_i|} \left( \frac{\partial \mathbf{B}_i^\top}{\partial \mathbf{r}} \mathbf{B}_i + \mathbf{B}_i^\top \frac{\partial \mathbf{B}_i}{\partial \mathbf{r}} \right) \right]. \quad (10) \end{aligned}$$

The three partial derivative terms can be calculated using an asymmetric rank one perturbation technique similar that shown in lemma 2 of [12]. The proof can be found in [13].

*Asymmetric rank one perturbations:* Let  $\alpha \in \mathbb{R}$ ,  $\mathbf{a}, \mathbf{b} \in \mathbb{R}^d$ , and  $\mathbf{X} \in \mathbb{R}^{d \times d}$  be an invertible matrix. Then if  $\alpha \neq -(\mathbf{b}^\top \mathbf{X} \mathbf{a})^{-1}$ , the rank one perturbed matrix  $\mathbf{X} + \alpha \mathbf{a} \mathbf{b}^\top$  is invertible and

$$(\mathbf{X} + \alpha \mathbf{a} \mathbf{b}^\top)^{-1} = \mathbf{X}^{-1} - \frac{\alpha \mathbf{X}^{-1} \mathbf{a} \mathbf{b}^\top \mathbf{X}^{-1}}{1 + \alpha \mathbf{b}^\top \mathbf{X}^{-1} \mathbf{a}}. \quad (11)$$

In addition, the perturbation determinant is

$$\det(\mathbf{X} + \alpha \mathbf{a} \mathbf{b}^\top) = (1 + \alpha \mathbf{b}^\top \mathbf{X}^{-1} \mathbf{a}) \det \mathbf{X}. \quad (12)$$

□

Therefore, by equation (11), the second term of equation (10) can be calculated for a perturbation of  $\mathbf{r}$  along any direction in the limit  $\alpha \rightarrow 0^+$ . Recall equation (6), and let  $\mathbf{A}_i = \mathbf{P}_i^{-1}$ . Then, for any element  $i$ ,

$$\begin{aligned} \frac{d\mathbf{B}_i}{d\alpha} &= \frac{d\mathbf{A}_i}{d\alpha} \Big|_{\setminus \text{row}1} \\ &= \frac{d}{d\alpha} \left[ (\mathbf{P}_i + \alpha \mathbf{a} \mathbf{b}^\top)^{-1} \right] \Big|_{\setminus \text{row}1} \Big|_{\alpha=0} \\ &= \left[ -\mathbf{P}_i^{-1} \mathbf{a} \mathbf{b}^\top \mathbf{P}_i^{-1} \right]_{\setminus \text{row}1} \\ &= \left[ -\mathbf{A}_i \mathbf{a} \mathbf{b}^\top \mathbf{A}_i \right]_{\setminus \text{row}1} \quad (13) \end{aligned}$$

and similarly

$$\frac{d\mathbf{B}_i^\top}{d\alpha} = \left( \frac{d\mathbf{B}_i}{d\alpha} \right)^\top = \left[ -\mathbf{A}_i^\top \mathbf{b} \mathbf{a}^\top \mathbf{A}_i^\top \right]_{\setminus \text{row}1}.$$

Table 1 FEM Forward & Inverse Model Pairs

Model pair	Elements		Nodes	
	Forward	Inverse	Forward	Inverse
A	7,680	1,536	1,595	369
B	15,360	3,072	3,045	697

The first term of equation (10) is calculated using equation (12):

$$\begin{aligned} \frac{d}{d\alpha} \frac{1}{|\det \mathbf{A}_i|} &= \\ &= \frac{-\text{sgn}(\det \mathbf{A}_i)}{\det \mathbf{A}_i^2} \frac{d}{d\alpha} \det \mathbf{A}_i \\ &= \frac{-\text{sgn}(\det \mathbf{A}_i)}{\det \mathbf{A}_i^2} \frac{d}{d\alpha} \det [(\mathbf{P}_i^{-1} + \alpha \mathbf{a} \mathbf{b}^\top)^{-1}] \Big|_{\alpha=0} \\ &= \frac{1}{|\det \mathbf{A}_i|} \mathbf{b}^\top \mathbf{A}_i \mathbf{a} \quad (14) \end{aligned}$$

Substituting equations (13) and (14) into (10) yields the sensitivity term for each element  $i$  with vertex represented by  $\mathbf{r}$

$$\begin{aligned} \frac{\partial \mathbf{S}_i}{\partial \mathbf{r}} &= \frac{2}{N_d!} \left[ \frac{1}{|\det \mathbf{A}_i|} \left( \mathbf{b}^\top \mathbf{A}_i \mathbf{a} \mathbf{B}_i^\top \mathbf{B}_i + \right. \right. \\ &\quad \left. \left. \frac{\partial \mathbf{B}_i^\top}{\partial \mathbf{r}} \mathbf{B}_i + \mathbf{B}_i^\top \frac{\partial \mathbf{B}_i}{\partial \mathbf{r}} \right) \right]. \quad (15) \end{aligned}$$

Equation (15) models the deformation of an element  $i$  incurred by the perturbation of the adjoining electrode with position vector  $\mathbf{r}$ . For each deformed element, the perturbations along  $x$ ,  $y$ , and  $z$  are calculated by choosing the unit vectors  $\mathbf{a}$  and  $\mathbf{b}$  in equations (13) and (14) that modify the corresponding node's coordinates. These coordinate data are stored as shown in equation (6). Thus, the FEM system matrix  $\mathbf{S}$  is constructed as in equation (5) where only the element blocks  $\mathbf{S}_i$  touching the displaced electrode are non-zero. Finally, the matrix  $\partial \mathbf{Y} / \partial \mathbf{r}$  can be directly computed, and the movement Jacobian is obtained by re-arranging the elements of  $\partial \mathbf{V} / \partial \mathbf{r}$  such that  $\mathbf{J}_m \in \mathbb{R}^{N_v \times 3N_e}$ .

### III. RESULTS

The computations of the conductivity distribution depend on quantities derived from the FEM geometry. Hence, we consider two model densities differing by a factor of 2: 1,536 and 3,072 elements, respectively. When simulating EIT data, we also rely on the FEM to solve the *forward problem*, i.e., calculating  $\mathbf{v}$  given  $\mathbf{S}$  and  $\boldsymbol{\sigma}$ . Table 1 summarizes the two FEM model pairs used, labeled A and B.

Image reconstructions were computed using the proposed method and were compared with the previously used indirect

Table 2 Movement Jacobian Results

Model pair	Computation Time (ms)		Relative Norm
	Direct	Indirect	$\ \mathbf{J}_{\text{indir}} - \mathbf{J}_{\text{dir}}\  / \ \mathbf{J}_{\text{dir}}\ $
A	840	22,420	$1.48 \times 10^{-6}$
B	1,460	41,430	$1.57 \times 10^{-6}$

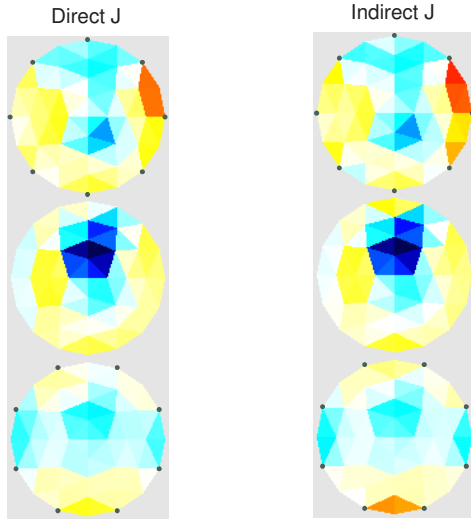


Fig. 2 Reconstructions of the FEM model in figure 1 using the direct and indirect methods.

perturbation method in [6]. Table 2 shows the average computation time required in milliseconds to compute the Jacobian matrix for each FEM model and the relative norm-error between both methods. A significantly longer computation time is required for the indirect method. The electrodes were slightly displaced (less than 1% of the model diameter) in simulations using the FEM model shown in figure 1. Figure 2 shows the reconstructions obtained with the direct and indirect methods. Three slices at  $z = -0.4, 0, +0.4$  are shown where the electrode positions are indicated by the small green circles. The position of both contrast elements in blue has been recovered; however, each method shows a slightly different artefact.

#### IV. DISCUSSION

In this study, we formulate a more efficient and accurate computation of the electrode movement Jacobian by eliminating the need of re-calculation of the forward problem and the numerical error associated with numerical perturbations. This was accomplished by implementing an asymmetric rank one perturbation technique similar to that described

in [12] directly on the FEM system matrix. The model developed here applies to point electrodes; however the underlying approach can be easily modified for use with more complex electrode models. Results show significantly faster computations that can complete a 15,000-element 3D FEM model with 16 electrodes in under 20 seconds using a standard desktop PC. Imaging results are similar to the previous, indirect method described in [6] and show no significant change in reconstruction fidelity. Such a calculation method may be useful in reconstruction algorithm design for large FEM inverse problems.

#### REFERENCES

- Lozano A, Rosell J, Pallás-Areny R (1995) Errors in prolonged electrical impedance measurements due to electrode repositioning and postural changes. *Physiol Meas* 16:121–130.
- Adler A, Guardo R, Berthiaume Y (1996) Impedance imaging of lung ventilation: do we need to account for chest expansion? *IEEE Trans Biomed Eng* 43:414–420.
- Blott BH, Daniell GJ, Meeson S (1998) Electrical impedance tomography with compensation for electrode positioning variations. *Phys Med Biol* 43:1731–1739.
- Lionheart WRB (1998) Boundary shape and electrical impedance tomography. *Inv Prob* 14:139–147.
- Kolehmainen V, Lassas M, Ola P (2005) The inverse conductivity problem with an imperfectly known boundary. *SIAM J Appl Math* 66:365–383.
- Soleimani M, Gómez-Laberge C, Adler A (2006) Imaging of conductivity changes and electrode movement in EIT. *Physiol Meas* 27:S103–S113.
- Polydorides N (2002) Image reconstruction algorithms for soft-field tomography. Ph.D. Thesis. University of Manchester Institute of Science and Technology pp.262.
- Graham BM, Adler A (2006) Electrode placement strategies for 3D EIT. 7th Conf Biomed EIT.
- Adler A, Lionheart WRB (2006) Uses and abuses of EIDORS: and extensible software base for EIT. *Physiol Meas* 27:S25–S42.
- Cheng KS, Isaacson D, Newell JC et al. (1989) Electrode models for electric current computed tomography. *IEEE Trans Biomed Eng* 36:918–924.
- Adler A, Guardo R (1996) Electrical impedance tomography: regularized imaging and contrast detection. *IEEE Trans Med Imag* 15:170–179.
- Olsen PA, Gopinath AR (2004) Modeling inverse covariance matrices by basis expansion. *IEEE Trans Speech Audio Processing* 12:37–46.
- Golub GH, Loan CFV (1996) Matrix computations. Johns Hopkins Univ. Press, Baltimore.

Address of the corresponding author:  
 Author: Camille Gómez-Laberge  
 Institute: Carleton University  
 Street: 1125 Colonel By Drive  
 City: Ottawa  
 Country: Canada  
 Email: cgomez@sce.carleton.ca